Advances in Natural Sciences:
Nanoscience and Nanotechnology

PAPER

Characterization of performance parameters of organic solar cells with a buffer ZnO layer

Adv. Nat. Sci.: Nanosci. Nanotechnol. **10** (2019) 015005 (5pp) https://doi.org/10.1088/2043-6254/aafda1

Characterization of performance parameters of organic solar cells with a buffer ZnO layer*

Nang Dinh Nguyen[1], Hyung-Kook Kim[2], Dinh Lam Nguyen[1], Duc Cuong Nguyen[1] and Phuong Hoai Nam Nguyen[1]

[1] Faculty of Engineering Physics and Nanotechnology, University of Engineering and Technology, Vetnam National University in Hanoi, E3-DHQGHN, 144 Xuan Thuy, Cau Giay, Hanoi, Vietnam
[2] Department of Nanoenergy, College of Nanoscience and Nanotechnology, Pusan National University, Samrangjin 1268–50, Samrangjin-eup, Miryang, Gyeong 50463, Korea

E-mail: dinhnn@vnu.edu.vn

Received 22 November 2018
Accepted for publication 25 December 2018
Published 31 January 2019

Abstract

By embedding a thin ZnO layer sandwiched between the hole transport and photoactive layers, organic solar cells (OSC) based on poly(3-hexylthiophene) (P3HT) were prepared by spincoating. UV–vis spectra of the composite films showed that ZnO exhibited a suitable buffer layer that could block holes movement throughout the heterojunction of ITO/ZnO. The enhancement in the fill factor (FF) of the buffer-OSC (BOSC) is attributed to the presence of nanoheterojunctions of ZnO/PCBM and ZnO/ITO. For the normal temperature, the increase of the open-circuit potential and short-circuit current resulted in an overall increase of the energy conversion efficiency. Comparing to OSCs without buffer layer (WOSC), the laminar structure of ITO/ZnO/P3HT/PCBM/Li/Al cells possess a much larger photovoltaic energy conversion efficiency, namely 2.12% (for BOSC) compared to 1.75% (for WOSC).

Keywords: buffer layer ZnO, energy bandgap, transmittance, organic solar cell, photoelectrical conversion efficiency
Classification numbers: 4.10, 4.11, 5.01, 5.10

1. Introduction

Inorganic solar cells like single-crystalline Si one have a large conversion efficiency, however they have limitations such as high costs imposed by fabrication procedures involving high temperature (500 °C to 1400 °C), high vacuum and lithography technology. Organic solar cells (OSC) that use polymers that can be processed from solution have been investigated as a low-cost alternative [1]. For many conjugated polymers, electron mobilities are low (10^{-4} cm^2 × V^{-1} × s^{-1}) due to the presence of numerous electron traps such as oxygen, vacancies. Moreover, the charge recombination or exciton decay results in reducing numbers of electrons and holes moving to opposite electrodes. Thus photoelectrical conversion efficiency (PCE) of OSCs is still much lower than that of Si-based solar cells. One way to overcome the charge recombination is to add a buffer layer like TiO_2, ZnO sandwiched between indium tin oxide (ITO) electrode and hole transport layer (HTL). As shown in [2], the transfer of the charges in organic devices can be improved by using both the inorganic semiconductor with a high electron affinity and conducting polymers with a low ionization potential. Among conducting polymers, poly(3-hexylthiophene) (P3HT) is used for flexible polymer electronic devices and OSCs. It is known that in a bulk heterojunction solar cell, P3HT with an energy bandgap of 1.9 eV [3] is often used as the electron donor and [6, 6]-phenyl C_{61}-butyric acid methyl ester (abbreviated to PCBM)—used as the acceptor [4, 5]. Comparing to C_{60}, PCBM has much better solubility in polymer that one can create a larger fullerene/conjugated polymer ratio, resulting in the formation of numerous donor–acceptor heterojunctions in OSCs [6]. Since the p-n junctions layers in organic device like OLEDs and OSCs can be easily prepared by spin-coating method, the production technology for either materials or devices of OSCs can be much reduced.

* Invited talk at 9th International Workshop on Advanced Materials Science and Nanotechnology (IWAMSN2018), 7-11 November 2018, Ninh Binh City, Vietnam

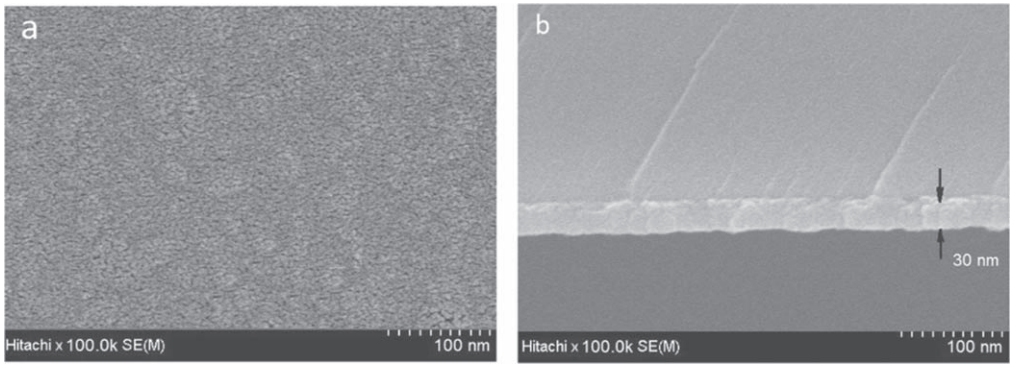

Figure 1. (a) SEM bright-field micrograph of the surface of ZnO/glass film. (b) SEM of a cross-section of the ZnO/glass film: the thickness of the ZnO layer is equal to approximately 30 nm.

In this work we demonstrate the advantage of using thin film of ZnO served as the buffer layer in OSCs in enhancement of the operating parameters of the devices. The comparison of these parameters of the devices without and with ZnO layer has been done.

2. Experimental

ITO-coated glass sheets with a sheet resistance of 10 Ω were used for substrates. The last was cleaned by ultrasonic stirring in distilled water, ethanol followed by acetone. The 30-nm thick ZnO layers were deposited onto glass (for optical properties characterization) and ITO-coated glass substrates (for making OSCs) by using magnetron Rf-sputtering (on Auto 500 Rf & Dc sputter coater), maintaining the substrate temperature at 450 °C. For the hole transport layer, a conjugate polymer of polyethylenedioxythiophene in poly(4-styrenesulfonate) (further shortly called PEDOT) with thickness of 70 nm was prepared. Spin-coating layers PEDOT/ITO and PEDOT/ZnO/ITO were made following techniques described in [6]. For the acceptor layer, a 50 nm-thick PCBM layer was spin-coated onto the PEDOT. Next, to deposit the photoactive layer onto PCBM/PEDOT, solution of P3HT was prepared from 8 mg P3HT powders dissolved in 1 ml of C_6H_5Cl (chlorobenzene). Next, this solution was spin-coated onto both the PCBM/PEDOT-PSS/ITO and the PCBM/PEDOT-PSS/ZnO/ITO. We have used the same experimental conditions as reported in [7], namely, first, the delay time was of 120 s, then the rest time of 30 s, the spin speed and the acceleration were chosen at 1500 rpm and 500 rpm, respectively. After completely drying in about 2 min, for the film polymerization the samples were annealed at 180 °C in dried gaseous nitrogen for 12 h. The P3HT obtained films were put on a Veeco Dektak 6 M stylus profilometer to measure the film thickness. The average value of the P3HT film thickness was found to be of 80 nm.

To prepare a good Ohmic contact between the metallic and the polymeric (P3HT) layers, a 20 nm-thick LiF/Al bilayer thin film was deposited onto the P3HT by vacuum evaporation as described in [8]. On the LiF/Al bilayer, an aluminum film with thickness of 70 nm was successively evaporated in a vacuum of 1.33×10^{-3} Pa, using a mask with windows of 3 mm × 3 mm in size (i.e. the active area of the device is of 0.09 cm^2). Thus two types of the OSCs were prepared, they have following laminar structure: (i) ITO/PEDOT/PCBM/P3HT/LiF/Al was abbreviated to WOSC, and (ii) ITO/ZnO/PEDOT/PCBM/P3HT/LiF/Al as BOSC. In WOSC there was absent the buffer layer, whereas in BOSC the ZnO layer plays the buffer role.

The surface morphology of samples was measured on a Hitachi field emission scanning electron microscopy (FE-SEM). X-ray diffraction (XRD) patterns were done on a Philips D-5005 diffractometer using filtered Cu-Kα radiation ($\lambda = 0.15406$ nm). The ultraviolet-visible transmittance spectra were carried out on a Jasco UV–vis-NIR V570. Measuring the performance parameters of the OSCs was carried-out on an AutoLab-Potentiostat PGS-30 electrochemical unit. The ITO side of the devices was illuminated with a power density of 100 mW×cm^{-2} by Sol 1 A Newport source which provides an energy spectrum similar to the solar one.

3. Results

The surface morphology of the ZnO films was revealed on the FE-SEM micrograph as shown in figure 1(a). The thickness of the ZnO film samples was determined by using the point-to-point marking technique in the SEM scanned at a cross-section of the ZnO/glass film (see figure 1(b)). The ZnO sample exhibited not completely uniform in the range of nanoscales, thus the average value of the ZnO film thickness was estimated about 30 nm (see figure 1(b)). To characterize the structure of ZnO film, we used XRD analysis. The XRD patterns of a ZnO/glass sample is presented in figure 2. From this figure one can find out that all six peaks observed in the XRD pattern belong to characteristic peaks of the ZnO crystal as reported in [9]. Those are the most intense peak of the (101) direction corresponding to $d = 0.253$ nm and five standard peaks of (100), (002), (102), (110) and (103) corresponding to $d = 0.284$, 0.263, 0.192, 0.163 and 0.149 nm. The XRD data obtained demonstrate that as-

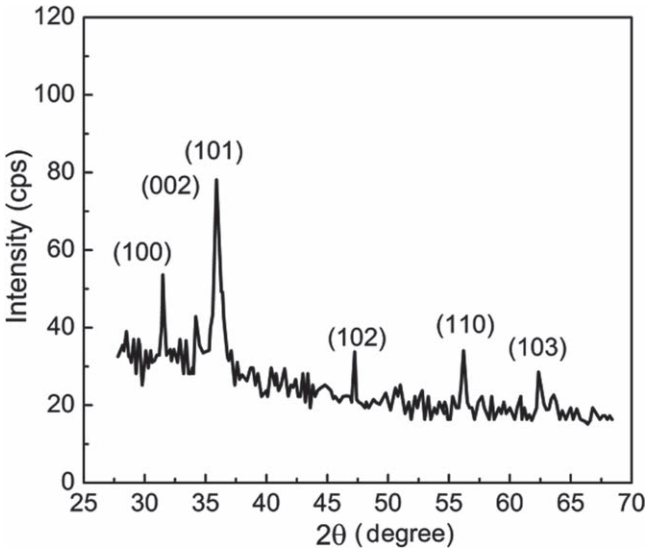

Figure 2. XRD pattern of an as-deposited (Rf-sputtering) ZnO film. Thickness $d = 30$ nm.

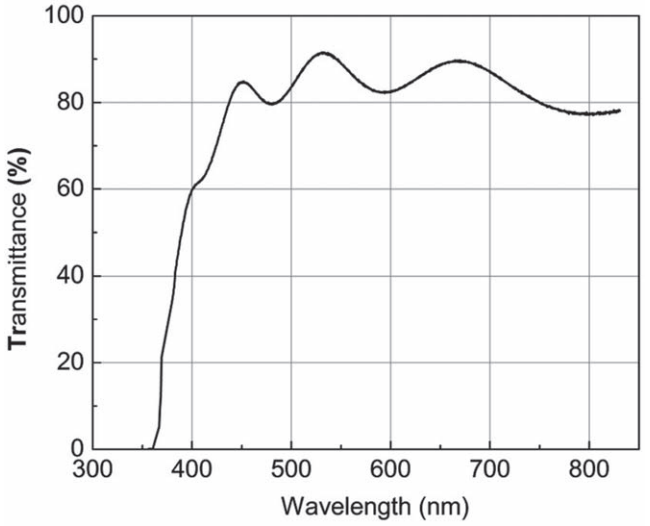

Figure 3. Transmittance spectrum of ZnO thin film. Thickness $d = 30$ nm.

deposited ZnO films by Rf-sputtering were well crystallized at 450 °C.

The transmittance spectra of both the ZnO/glass and ZnO/ITO samples were measured with baseline regime for the elimination of the glass and ITO/glass absorption. Figure 3 shows the transmittance spectrum obtained for ZnO/glass. The wave-like shape of the spectrum is explained due to the interference effect that occurred on the thin film coated on glass. The largest absorptance was observed at short wavelengths (from 360 to 400 nm).

As reported in [10], the energy bandgap (E_g) of a semiconducting oxide film can be determined by using its UV–vis spectra. Basing on the calculation way described in [9], we estimated the value of the bandgap of ZnO film using the following expression:

$$\alpha(\nu)h\nu = A(h\nu - E_g)^n, \tag{1}$$

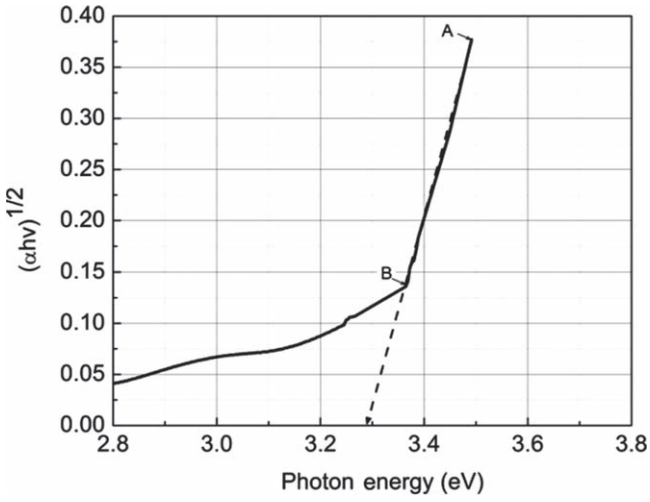

Figure 4. Plot of $(\alpha h\nu)^{1/2}$ Versus Photon energy ($h\nu$) for the determination of E_g of ZnO film.

where $\alpha(\nu)$ is the absorptance versus the frequency, h is Planck's constant, ν is the frequency of the incident UV–vis radiation, A is a constant and n is $1/2$ for direct band semiconductors and 2 for indirect band gap semiconductors. As shown in [11], if the reflectance of the films is too small that can be ignored, one can express $\alpha(\nu)$ through the optical transmittance spectra (T) as follows:

$$\alpha(\nu) = \frac{1}{d}\ln\left(\frac{1}{T}\right). \tag{2}$$

We have plotted the photon energy dependence of $\alpha(\nu)$ for both $n = 1/2$ and $n = 2$ and noted that the best fit was $n = 2$ (corresponding to the indirect bandgap). This plot is shown in figure 4. From this figure one can see that the line segment 'A-B' is a linear $h\nu$-dependence of $(\alpha h\nu)^{1/2}$. Thus the line A-B crosses the abscissa at the value of the photon energy (namely $h\nu$), that is the energy bandgap (E_g) of the material. As seen in figure 4, the cross point is at $h\nu = 3.28$ eV, consequently the bandgap of ZnO film $E_g = 3.28$ eV. This value is quite close to E_g of ZnO crystal [12].

The obtained result proves that the ZnO thin film has a large energy bandgap. Since ZnO has the relative bandgap structure with ITO and PCBM:P3HT at the heterojunctions as shown in figure 5, one can use it for the buffer layer (BL) in the organic solar cells. Due to the BL, the holes are blocked at the ZnO/PCBM interface, resulting in reduction of the exciton decay. The charge separation thus can be enhanced with the addition of the buffer ZnO layer. As shown in [13], according to the energy level of ZnO compared to that of ITO and PCBM , one can see that at the ZnO/PCBM interace there exists a very small difference between conduction band energy levels E_c of ZnO and PCBM. On the contrary, there is a large difference between their valence band energy levels E_v. This means that the energy barrier for electrons is negligible, whereas for holes it is very large. This is the reason why adding the buffer layer and adjacent electrodes with Ohmic contacts, one can raise the internal electrical field

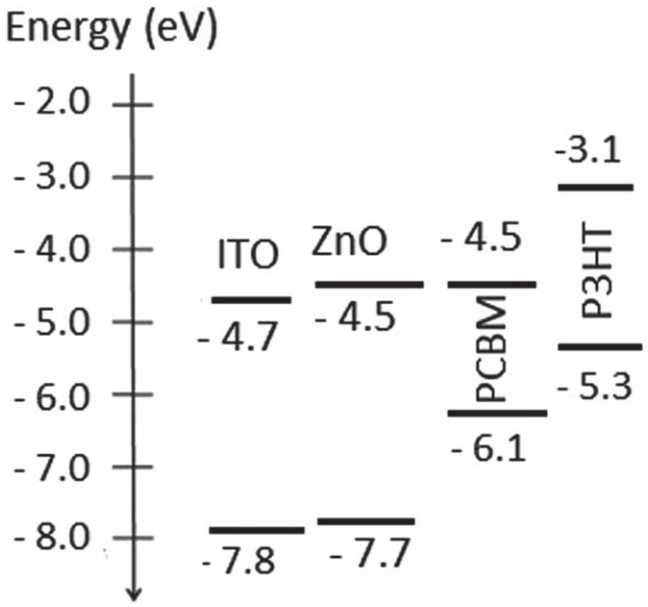

Figure 5. Schematic energy levels of ITO, ZnO, PCBM and P3HT; ZnO blocks holes and acts as electron transport buffer layer.

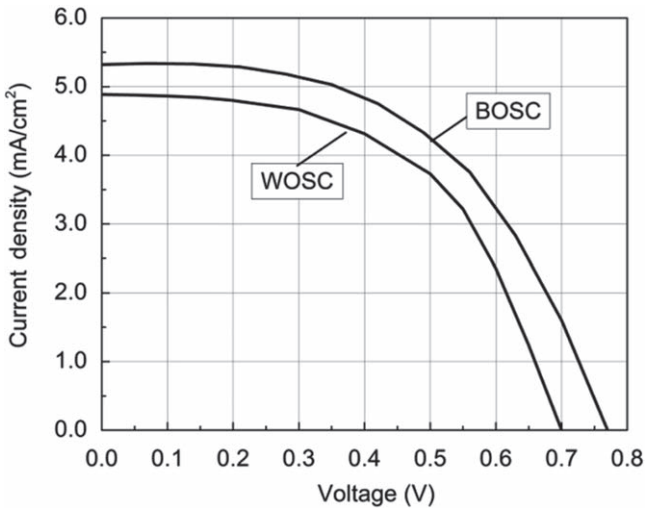

Figure 6. $J - V$ characteristics obtained in the illumination regime for the cells with the structure of ITO/PEDOT/P3HT:PCBM/LiF/Al (WOSC) and ITO/ZnO/PEDOT/P3HT:PCBM/LiF/Al (BOSC).

Table 1. Performance parameters of WOSC and BOSC solar cells.

Device	V_{oc}(mV)	J_{sc}(mA cm^{-2})	*FF*	η(%)
WOSC	700	4.88	0.46	1.75
BOSC	770	5.32	0.52	2.12

intensity, resulting in increase in the open-circuit voltage V_{oc} of the cell.

From the measurement of the performance of two devices WOSC and BOSC one can get J–V curves in dark and illuminated regimes. From the $J - V$ curves we calculated the values of all parameters of the devices, such as fill factor (*FF*), open-circuit voltage (V_{oc}), short-current density (J_{sc}) and photoelectrical conversion efficiency (η). In fact, there is a competition between charge carrier recombination and transport. The *FF* can be determined by formula

$$FF = \frac{(JV)_{\max}}{J_{sc}V_{oc}}, \tag{3}$$

where $(JV)_{\max}$ is the largest area of the rectangle. Thus η can be determined by:

$$\eta = \frac{FF\ J_{sc}V_{oc}}{P_{\text{in}}}, \tag{4}$$

where P_{in} is the density of the illuminating power (in our experiments $P_{\text{in}} = 100\,\text{mW} \times \text{cm}^{-2}$). To determine the experimental performance parameters of both the WOSC and BOSC as V_{oc}, J_{sc} and *FF*, we measured the voltage dependence of the current density ($J - V$) by using the cyclic voltammetry on the Auto-Lab. Potentiostat PGS-30 (as shown in the experimental session) for both the dark and illumination regime. Herein $J - V$ curves in the dark regime are not showed. The $J - V$ curves for two types of the OSCs shown in figure 6 revealed the current-voltage ($J - V$) characteristics of WOSC and BOSC, under an illumination with a power density of $100\,\text{mW} \times \text{cm}^{-2}$.

The fill factor and photoelectrical conversion efficiency (PCE) which were calculated by equations (3) and (4), together with V_{oc} and J_{sc} taken from the $J - V$ curves are displayed in table 1. Both V_{oc} and J_{sc} of the BOSC cell have a larger value than that of WOSC (namely 770 mV versus 700 mV for V_{oc} and 5.32 mA versus 4.88 mA for J_{sc}). The fact that the *FF* of the BOSC is larger than that of WOSC proves that the ZnO layer exhibited a good hole blocking layer. This results in an increase of the J_{sc}, and consequently the efficiency (η) of the device containing the ZnO buffer layer. As shown in [14], under AM1.5 illumination the dye sensitized solar cells (DCCSs) possess a photoelectrical conversion efficiency (η) as large as 8.86%. Comparing to the DSSCs, η of our OSCs (namely BOSC device) is still small (i.e. $\eta = 2.12\%$). But this value is well comparable to the one of the solid-state photovoltaic devices made from the surface-adsorbed dye complex for light absorption and electron injection to the TiO_2 layer, used for *n*-type and the *p*-type semiconductors, respectively [15].

4. Conclusion and discussion

Thin ZnO films on glass and ITO-coated glass substrates were deposited by using magnetron Rf-sputtering. Characterization of the morphology, crystalline structure and optical properties of ZnO films showed that the 30-nm thick ZnO films were suitable for using as the buffer layer sandwiched between the hole transport and photoactive layers in organic solar cells.

The enhancement in the performance parameters of the buffer-OSCs was explained due to the presence the ZnO buffer layer that created two nanoheterojunctions of ZnO/PCBM and ZnO/ITO. The laminar structure of the cells with the ZnO buffer layer of ITO/ZnO/P3HT/PCBM/LiF/Al

(BOSC) possess much larger photovoltaic energy conversion efficiency in comparison with OSCs without buffer layer (WOSC), namely 2.12% (for BOSC) compared to 1.75% (for WOSC).

Although the photoelectrical conversion efficiency of the BOSC device is in 21%, i.e. (2.12%−1.75%)/1.75% larger than that of WOSC devices, its absolute value is not large. One can mention two of the reasons resulting in the efficiency limitaton as follows. Firstly, the P3HT/PCBM junctions are planar, not bulk heterojunctions (BHJ) formed by embedding PCBM nanoparticles in P3HT (P3HT:PCBM) [16]. The second, in our devices there are neither antireflection coatings nor metallic nanoparticles resulting in the plasmonic enhancement in light trapping which is a hightly efficient method for the enhancement of the PCE in polymer solar cells, as analyzed in a recent work of Nguyen *et al* [17].

Acknowledgments

This research was funded by the grant of Vietnam National University Hanoi (VNUH) in period of Y2018–2020 (Code No.: QG.19.20). The author (N D N) expresses his sincere thanks to the College of Nanoscience and Nanotechnology, Korea Pusan National University for strongly supporting the colaboration between the COE of Prof. Dinh and Prof. Kim's Laboratory.

References

[1] Huynh W U, Dittmer J J and Alivisatos A P 2002 *Science* **295** 2425
[2] Greenham N C, Peng X G and Alivisatos A P 1996 *Phys. Rev.* B **54** 17628
[3] Ren S, Chang L Y, Lim S K, Zhao J, Smith M, Zhao N, Bulovic V, Bawendi M and Gradecak S 2011 *Nano Lett.* **11** 3998
[4] Gelinck G H, Warman J and Staring E G J 1996 *J. Phys. Chem.* **100/13** 5485
[5] Hummelen J C, Knight B W, Lepec F and Wudl F 1995 *J. Org. Chem.* **60** 532
[6] Katz E A, Faiman D and Tuladha S M 2001 *J. Appl. Phys.* **90/10** 5343
[7] Thao T T, Trung T Q, Vo-Van T and Dinh N N 2015 *J. Nanomat.* **2015** 463565
[8] Dinh N N, Chi L H, Thuy T T C, Trung T Q and Vo-Van T 2009 *J. Appl. Phys.* **105** 093518
[9] Fierro J L G (ed) 2006 *Metal Oxides: Chemistry and Applications* (Boca Raton, FL: CRC Press) p 182
[10] Kim Y, Choulis S A, Nelson J, Bradley D D C, Cook S and Durrant J R 2005 *Appl. Phys. Lett.* **86** 063502
[11] Meneses-Rodríguez D, Horley P P, González-Hernández J, Vorobiev Y V and Gorley P N 2005 *Solar Energy* **78** 243
[12] Kiyoshi T, Akihiko Y and Adarsh S (ed) 2007 *Wide Bandgap Semiconductors: Fundamental Properties And Modern Photonic And Electronic Devices* (Berlin Heidelberg: Springer) p 357
[13] Hori T, Moritou H, Fukuoka N, Sakamoto J, Fujii A and Ozaki M 2010 *Materials* **3** 4915
[14] Chandrasekhar P S, Parashar P K, Swami S K, Dutta V and Komarala V K 2018 *Phys. Chem. Chem. Phys.* **20** 9651
[15] Kaiser K E, Fischer C H, Kfnenkamp R, Rost C, Sieber I and Ch L-S M 2001 *Sol. Energy Mater. Sol. Cells* **67** 89
[16] Ostfeld A E and Pacifici D 2011 *Appl. Phys. Lett.* **98** 113112
[17] Nguyen B H, Nguyen V H and Vu D L 2015 *Adv. Nat. Sci.: Nanosci. Nanotechnol.* **6** 043002